THE ORIGIN OF FILAMENTS IN EXTENDED RADIO SOURCES

Elisabete M. de Gouveia Dal Pino and Reuven Opher
Instituto Astronômico e Geofísico, Universidade de São Paulo
Received 1987 April 21; accepted 1988 November 3

ABSTRACT

Are the recently observed filaments in extended radio sources due to a thermal instability? This is the question addressed in the present paper. Using luminosities, pressures, and expansion rates indicated by observations of extended radio sources, we make a linear and nonlinear analysis of thermal instability in these sources. We study a model in which the unknown (as yet) process which creates approximate equipartition in extended radio sources does no act continuously, but ceases for time intervals $\sim R/V_R$, where R is the radius of the extended radio source and V_R is the radial expansion velocity. We show that the maximum value of $q = V_A^2/V_S^2$ under isobaric conditions for thermal instability is $q_0 = [-2v_e + (\frac{3}{4}\tau_c)(2\eta - 1)]/[(2v_e/3) + (2/\tau_c)]$, where $V_A(V_S)$ is the Alfvén (sound) velocity, $v_e \equiv V_R/R$, $\tau_c \equiv 3P/L_{sc}$, with L_{sc} the total synchrotron and inverse Compton losses, $\eta = [1 + (8\pi U_{rad}/B^2)]^{-1}$, with U_{rad} the energy density of the background radiation, B the magnetic field, and P the pressure due to the relativistic electrons. Nonlinear calculations with initial density perturbations $[\rho_p(0) - \rho_0(0)]/\rho_0(0) = 0.05, 0.1, 0.2$, and 0.3 were made, and it was found that the maximum density contrast $\rho_p(t)/\rho_0(t)$ was approximately independent of the initial density perturbation, where $\rho_p(t)[\rho_0(t)]$ is the perturbed (ambient) density at time t. The maximum nonlinear emissivity contrast was also found to be independent of inverse Compton losses, opposite to results in the linear regime where inverse Compton losses suppress thermal instability. For the inner jet of Cen A, using observed and estimated values of R, V_R, L_{sc}, and P in the region of the A1 knot, we find that thermal instability creates a density contrast $\rho_p(t)/\rho_0(t) \sim 6$–$8.4$ in a distance comparable to the separation distance of the A1 and A4 knots, sufficient to explain the observed filaments. Applying our analysis to the region where the jet enters the radio lobe of Cyg A, we find that thermal instability creates a density contrast $\rho_p(t)/\rho_0(t) \sim 2$–$5$ in the estimated lifetime of Cyg A which, again, is sufficient to explain the observed filaments.

Subject headings: galaxies: jets — hydromagnetics — instabilities — radiation mechanisms — relativity

I. INTRODUCTION

A general discussion of various types of thermal instabilities that can be important in astrophysical phenomena was given by Field (1965). Recent observational evidence of filamentary structure in radio jets (e.g., Cen A; Clarke, Burns, and Feigelson 1986), radio lobes (e.g., Cyg A; Perley, Dreher, and Cowan 1984), and detection of optical emission (continuum and line) (assumed to be emitted by clumps or filaments inside the inner jet of Cen A in the region between the A1 and B knots; e.g., Brodie, Königl, and Bowyer 1983; Brodie and Bowyer 1985) are indications that thermal instabilities may be important in extended radio sources.

Simon and Axford (1967), interested in the filamentary structure of the Crab Nebula, made a linear study of the thermal instability (TI) of a static and homogeneous medium with a relativistic electron gas heated per unit volume at a constant rate and subject to synchrotron and inverse Compton losses.

Eilek and Caroff (1979) made a linear analysis of a static and homogeneous medium of dynamically dominant relativistic electrons and a warm inertial gas, subject to bremsstrahlung, Coulomb, synchrotron, and inverse Compton losses. They found that plasmas in which the cooling is dominated by the first two processes are generally unstable, that synchrotron losses may or may not cause instability, and inverse Compton losses, in general, are stabilizing. For extended radio sources (ERS), bremsstrahlung and Coulomb losses are, in general, less important than synchrotron and inverse Compton losses.

Marscher (1980) discussed TI in compact sources, neglecting the presence of a background thermal plasma. In his numerical calculations Marscher assumed either no expansion and no magnetic pressure ($q = 0$, $v_e = 0$) (Marscher's Fig. 1), no expansion and a magnetic pressure 3×10^{-3} that of the relativistic electrons ($q \cong 10^{-3}$, $v_e = 0$) (Marscher's Fig. 2), or $v_e \tau_S = 1/8.7 = 0.11$, with $q = 0$ or $q \cong 10^{-3}$ (Marscher's Fig. 3), where $q \equiv V_A^2/V_S^2$, V_A is the Alfvén velocity, V_S is the sound velocity, v_e is the expansion rate, $v_e \equiv V_R/R$, $\tau_S \equiv l/V_S$, and l is the radius of the perturbed volume, R is the radius of the ERS, and V_R is the radial expansion velocity. He assumed initial magnetic perturbations $\epsilon \equiv (B_p - B_0)/B_0 = 0.1, 0.2, 0.3$, and 0.4 (Marscher's eq. [(16)], where $B_p(B_0)$ is the magnetic field of the perturbed (ambient) region. He found for the expansion rate studied ($v_e \tau_S = 0.11$) that the perturbation $\epsilon = 0.1$ does not grow (Marscher's Fig. 3). Marscher (1980) used in his calculations the synchrotron cooling time $\tau_c[\propto (B^2\bar{E})^{-1}]$, with a fixed average energy $\bar{E} = 940$ MeV. This makes $\tau_c \propto B^{-2}$.

Recent observational data on radio jets and lobes give appreciable information on the values and functional dependences of the important parameters of the thermal instability: q, τ_c, and v_e. For example, the minimum pressure is determined by equipartition P_{eq} (where $q = q_{eq} = 9/8$). For a given luminosity, the ambient electron pressure, P_0, for small B varies as $B^{-3/2}$ (Burns, Owen, and Rudnick 1979). Since $q \propto B^2/P_0$ for B small, $P_0 \propto q^{-3/7}$. Thus the values of $q = 0$ and $q = 10^{-3}$ used by Marscher (1980) for compact radio sources correspond to $P_0/P_{eq} \cong \infty$ and $P_0/P_{eq} \cong [10^{-3}/(9/8)]^{-3/7} \cong 20$. But P_{eq} is already on the order of the upper

686

limit of the external pressure determined by X-ray data for ERS. This is thus evidence against the values of $q \cong 0$ and $q \cong 10^{-3}$ for ERS.

Observational data also give information on the cooling time τ_c. We have $\tau_c = 3P_0/L_{sco}$, where L_{sco} is the synchrotron plus inverse Compton losses of the ambient region. The indicated relatively slow dependence with distance of P_0 from the X-ray data, and the slow dependence with distance of L_{sc} from the radio-optical radiation data, probably eliminates the possible dependence $\tau_c \propto B^{-2}$ used by Marscher (1980), resulting from using a fixed average energy $\bar{E}$.

In the present paper, we do not use a fixed $\bar{E}$, but obtain τ_c from the spatial dependence of the observed luminosity. Our model avoids assuming excessively large values of P_0. For Cen A, for example, we begin our calculation with $P_0 = 1.0 \times 10^{-10}$ dynes cm^{-2} and at the time of the maximum condensation of the nonlinear calculation we have $P_0 \cong 7.9 \times 10^{-11}$ dynes cm^{-2}. For Cyg A, we start with $P_0 = 5 \times 10^{-11}$ dynes cm^{-2}, and at the maximum condensation we have $P_0 \cong 7.5 \times 10^{-11}$ dynes cm^{-2}. The expansion rates studied in the present paper are taken from the observations of Cen A and Cyg A.

Are the recently observed filaments in ERS, such as in Cen A and Cyg A, due to TI? This is the question addressed in the present paper. Using expansion rates, luminosities of ERS, and $P_0 \sim 0.5$–1×10^{-10} dynes cm^{-2} indicated by observations, we make a linear and nonlinear analysis of TI in ERS. We study a model in which the unknown (as yet) process which creates approximate equipartition in ERS does not act continuously, but ceases for time intervals $\sim R/V_R$, where R is the radius of the ERS and V_R is the radial expansion velocity.

In the present paper, we attempt to answer the following questions:

1. Can the luminosities, pressures, and expansion rates inferred from observational data and energy considerations produce thermal instabilities in radio jets and lobes?

2. If so, are the instabilities sufficiently strong to produce the filaments observed in the inner radio jet of Cen A (e.g., Clarke, Burns, and Feigelson 1986) and the radio lobe of Cyg A (e.g., Perley, Dreher, and Cowan 1984)?

3. Do the expansion rates put a lower limit on the smallest possible initial perturbed magnetic field? For example, is $\epsilon \equiv (B_p - B_0)/B_0 \lesssim 0.1$ possible?

4. What are the indicated density contrasts for developed thermal instabilities?

The layout of the paper is as follows. Sections II and III discuss the model and the basic equations. Section IV discusses the linear equations. In § V, we discuss the nonlinear equations of the model, and in § VI and VII we present the results of our calculations and our conclusions.

II. THE MODEL

The major part of the internal energy of the system (and the pressure) is by assumption due to the relativistic electrons emitting synchrotron and inverse Compton radiation. A cold component of the gas, although containing a negligible internal energy, provides the major part of the mass density and inertia of the system. We restrict the analysis to transverse perturbations to the magnetic field, since the growth of longitudinal perturbations tends to be inhibited by the thermal conductivity of the relativistic component, which is very large parallel to the magnetic field. We assume that both gas components are physically coupled such that they have the same macroscopic velocity and move jointly in any perturbation. The magnetic field lines are assumed to be frozen into the plasma. In our model, the reference system is a volume element of plasma moving along the z-axis of a jet with the velocity V_J (i.e., the velocity of the fluid along the axis). In this reference system, the parameters of the plasma are functions only of the cylindrical transverse coordinate, r, and the time $t = z/V_J$ (assuming azimuthal symmetry). The magnetic field $\boldsymbol{B}$ is assumed to be parallel to the z-axis of the jet, the border of which describes a cone of constant opening angle θ, such that the transverse velocity V_R of the border of the jet is given by $V_R = V_J \tan \theta$.

We assume, similar to previous calculations, that the gain function G (i.e., the heating rate per unit volume of the hot component) is independent of the local physical parameters, i.e., $G_1 \equiv G_p - G_0 = 0$ (e.g., Simon and Axford 1967), where $G_p(G_0)$ is the gain function for the perturbed (ambient) region. It is difficult to improve on this assumption since the nature of the heating or acceleration of the relativistic particles is still uncertain, in particular, in the internal regions far from the surface (see, however, Gouveia Dal Pino and Opher [1989] for the study of a more general G).

For the evaluation of the energy losses of the plasma due to synchrotron radiation of the relativistic electrons, we assume (similar to Simon and Axford 1967) that the distribution of the electrons is isotropic and given by a relativistic Maxwellian distribution characterized by an average energy per particle E, such that the pressure is given by $P = nE/3$, where n is the numerical density of the relativistic electrons.

The synchrotron loss function is

$$L_s = a_s n B^2 E^2 \text{ ergs cm}^{-3} \text{ s}^{-1} , \tag{1}$$

where $a_s = 2.11 \times 10^{-3}$ in cgs units.

Similar to Simon and Axford (1967) and Marscher (1980), we assume a Maxwellian distribution to evaluate L_s, knowing that the emitted synchrotron radiation indicates a power-law distribution. Although the two distributions are formally different, what is primarily important is the ratio $3P/L_s$, which defines the electron cooling time τ_c, and is the same for both distributions.

We also include in our calculations inverse Compton losses due to the microwave background. Since inverse Compton and synchrotron losses have the same functional dependence on E they can be written together, resulting in a total loss function for the relativistic electrons

$$L_{sc} = a_s n E^2 (B^2 + B_c^2) , \tag{2}$$

where

$$B_c = (8\pi U_{rad})^{1/2} \tag{3}$$

is the equivalent magnetic field of the ambient radiation field of energy density U_{rad}. In this paper, we consider only the minimum inverse Compton losses that come from the background cosmological radiation

$$B_c = 3.2 \times 10^{-6}(1 + Z)^2 \text{ G} \qquad (4)$$

(de Young 1976), where Z is the redshift of the source. In general, for ERS, the U_{rad} for the cosmological background radiation is greater than that of the synchrotron radiation.

Defining

$$\eta \equiv B^2/(B^2 + B_c^2) \qquad (5)$$

(e.g., Eilek and Caroff 1979), we can write equation (2) in the form

$$L_{sc} = a_s nE^2 B^2/\eta = c_s B^2 P^2/n\eta , \qquad (6)$$

where $c_s = 9a_s = 1.89 \times 10^{-2}$ in cgs units.

Let us evaluate the emissivity contrast to compare with observations. A major part of the particles may be in the observed filaments. Let us assume that a fraction $1 - F$ of the total number of particles is in the observed filaments (and a fraction F in the ambient region). The factor $1 - F$ is similar to the frequently used filling factor, the principal difference being that the filling factor is the fraction of the total volume occupied by the filaments, while $1 - F$ is the fraction of the total number of particles in the filaments. We designate ρ_0, P_0, and L_{s0} as the density, electron pressure, and synchrotron emissivity, respectively, of an ambient region unperturbed by the formation of filaments, and $\bar{\rho}_0$, $\bar{P}_0$, and $\bar{L}_{s0}$ the respective quantities of the actual ambient region. The approximate relation between the emissivity contrast $L_{sp}/\bar{L}_{s0}$ between the synchrotron emissivity of the perturbed region and the actual ambient region and ρ_p/ρ_0 (the calculated density contrast between the perturbed region and the unperturbed ambient region) and P_p/P_0 (the calculated electron pressure contrast between the perturbed region and the unperturbed ambient region) can be obtained as follows. In the ambient region the electron pressure dominates the magnetic pressure. Since the condensation process occurs in approximate isobaric conditions (see below) we have $P_0 \sim \bar{P}_0$. In our model $B \propto n \propto \rho$, and we obtain from equation (1)

$$\frac{L_{sp}}{\bar{L}_{s0}} \cong \left(\frac{\rho_p}{\rho_0}\right)\left\{\frac{1 - [(1 - F)/(\rho_p/\rho_0)]}{F}\right\}\left(\frac{P_p}{P_0}\right)^2 . \qquad (7)$$

Marscher (1980), in his analysis of the thermal instability, assumed a square density profile of the perturbation (e.g., eq. [17], Marscher 1980) and perturbations in the form of spheres of initial radius l. In the present analysis, due to the presence of the magnetic field, we believe that a cylindrically symmetric perturbation and a smooth decreasing density profile are more appropriate. We thus assume cylindrical symmetry and our perturbed volume has a filamentary structure, long in the z-direction and narrow in the r-direction. We assume for the transverse velocity of the perturbed region $v_{1r}(r, t)[= v_r(r, t) - v_{0r}(r, t)]$ a sine distribution

$$v_{1r}(r, t) = \hat{v}_1(t) \sin kr , \qquad (8)$$

with $v_{0r}(r, t)$ having the dependence

$$v_{0r}(r, t) = V_R r/R(t) , \qquad (9)$$

$$V_R \equiv V_J \tan \theta , \qquad (10)$$

where $R(t)$ is the radius of the jet. The velocities v_{1r} and v_{0r} satisfy the boundary condition of continuity in cylindrical symmetry, $v_{1r}(0, t) = v_{0r}(0, t) = 0$. Instead of the square density profile used by Marscher (Marscher 1980 eq. [17]), we use a cosine distribution,

$$\rho_1(r, t) = \hat{\rho}_1(t) \cos kr , \qquad (11)$$

up to the radius of the filament

$$\bar{r}(t) = \pi/2k(t) , \qquad (12)$$

where $\rho_1(\bar{r}, t) = 0$. We also assume B_1 and $P_1 \propto \cos kr$ up to $\bar{r}$ (eq. [12]). The wave number $k(t)$ [$\gg R^{-1}(t)$] in equation (12) is determined by the conservation of magnetic flux:

$$\int_0^{\bar{r}(t)} \{B_0(t) + \hat{B}_1(t) \cos [k(t)r]\}r\, dr = \int_0^{\bar{r}(0)} \{B_0(0) + \hat{B}_1(0) \cos [k(0)r]\}r\, dr . \qquad (13)$$

As mentioned above, we assume that the unknown (as yet) process which creates equipartition in radio sources does not act continuously, but ceases for times $\sim R/V_R$. Since $q(\propto B^2/P)$ decreases with increasing R, q will decrease from $q_{eq} = 9/8$ to the value q_0 where the thermal instability can begin. We evaluate q_0 and start our calculations from $q = q_0$.

FILAMENTS IN EXTENDED RADIO SOURCES

III. BASIC EQUATIONS

The basic equations to be solved are

$$\frac{d\rho}{dt} + \rho \nabla \cdot \boldsymbol{v} = 0 , \tag{14}$$

$$\rho \frac{d\boldsymbol{v}}{dt} + \nabla\left(P + \frac{B^2}{8\pi}\right) = \frac{1}{4\pi}(\boldsymbol{B} \cdot \nabla)\boldsymbol{B} , \tag{15}$$

$$\frac{d\boldsymbol{B}}{dt} + \boldsymbol{B}(\nabla \cdot \boldsymbol{v}) = (\boldsymbol{B} \cdot \nabla)\boldsymbol{v} , \tag{16}$$

$$\frac{1}{\Gamma - 1}\frac{dP}{dt} - \frac{\Gamma}{\Gamma - 1}\frac{P}{\rho}\frac{d\rho}{dt} + \mathcal{L} = 0 , \tag{17}$$

and the equation of state

$$P = \frac{1}{3} nE , \tag{18}$$

where ρ is the mass density, $\boldsymbol{v}$ is the macroscopic transverse velocity of the plasma, $d/dt = \partial/\partial t + (\boldsymbol{v} \cdot \nabla)$, P is the pressure entirely due to the relativistic component, n the numeric density of the relativistic electrons of average energy E, Γ is the ratio of the specific heats, $\mathcal{L} \equiv L - G$, where L is the energy loss, and G is the energy gain per unit volume per second. We assume L is entirely due to losses by synchrotron and inverse Compton radiation, L_{sc}.

We assume the energy gain of the relativistic particles G is given by an unspecified mechanism (e.g., MHD waves) and independent of the local physical variables. A possible interpretation (Eilek and Caroff 1979) of a G-function independent of the local variables is that the perturbed region is optically thick, absorbing all the incident energy, independent of the physical parameters within the region. (Elsewhere [Gouveia Dal Pino and Opher 1989], we investigate the thermal instability for a G function that is dependent on the local variables, assuming the relativistic electrons are reaccelerated by resonant interaction with Alfven waves, based on the work of Eilek and Henriksen 1984.)

IV. LINEAR EQUATIONS

We first examine the effect of small perturbations, assuming that the perturbed quantities v_1, ρ_1, B_1, and P_1 (eqs. [8]–[11]) are small compared with the unperturbed quantities v_0, ρ_0, B_0, and P_0, respectively. The magnetohydrodynamic equations (14)–(18) then yield two sets of equations, a zeroth-order set and a first-order set. The zeroth-order set gives

$$\rho_0(t) = \rho_0(0)[R(0)/R(t)]^2 , \tag{19}$$

$$B_0(t) = B_0(0)[R(0)/R(t)]^2 , \tag{20}$$

$$n_0(t) = n_0(0)[R(0)/R(t)]^2 , \tag{21}$$

and

$$\dot{P}_0(t) = -2\Gamma P_0 v_e(t) - (\Gamma - 1)[L_{sco}(t) - G_0(t)] . \tag{22}$$

where $\Gamma = 4/3$ is the ratio of the specific heats of the relativistic gas and v_e is the expansion rate of the jet

$$v_e = \frac{\dot{R}(t)}{R(t)} = \frac{V_R}{R(t)} . \tag{23}$$

Unlike previous works (e.g., Simon and Axford 1967; Eilek and Caroff 1979), we do not assume the thermal balance between the gain and the loss functions in the equilibrium state, $G_0 = L_{sco}$. In the present model, since the gain function $G_0(t)$ is unknown and is assumed to be independent of the local variables of the perturbed region, we cannot obtain $\dot{P}_0(t)$ directly from equation (22). However, we can determine from the observations a semi-empirical function for $L_{sco}(t)$ and according to equations (1), (18), (20), and (21),

$$P_0(t) = P_0(0)\left[\frac{L_{s0}(t)}{L_{s0}(0)}\right]^{1/2} \frac{R(t)}{R(0)} , \tag{24}$$

where $L_{s0}(t) = L_{sco}(t)\eta_0$. Equation (22), then, can be used to determine $G_0(t)$.

By linearizing the variables in the above way, we allow for the possibility that the unperturbed quantities may vary by large factors, and the resulting linearized equations will still be valid provided that the spatial perturbations are small.

The first-order equations for $\hat{\rho}_1(t)$, $\hat{v}_1(t)$, $\hat{B}_1(t)$, and $\hat{P}_1(t)$ are

$$\dot{\hat{\rho}}_1(t) = -\rho_0 \bar{k} \hat{v}_1(t) - 2\nu_e \hat{\rho}_1(t) , \tag{25}$$

$$\dot{\hat{v}}_1(t) = \frac{k}{\rho_0}\left[\hat{P}_1(t) + \frac{B_0}{4\pi}\hat{B}_1(t)\right] - \nu_e \hat{v}_1(t) , \tag{26}$$

$$\dot{\hat{B}}_1(t) = -B_0 \bar{k} \hat{v}_1(t) - 2\nu_e \hat{B}_1(t) , \tag{27}$$

$$\dot{\hat{P}}_1(t) = -\frac{4}{3} P_0 \bar{k} \hat{v}_1(t) + \frac{3}{4}\frac{V_S^2}{\tau_c}\hat{\rho}_1(t) - \left(\frac{8}{3}\nu_e + \frac{2}{\tau_c}\right)\hat{P}_1(t) - \frac{2}{3}L_{s0}\frac{\hat{B}_1(t)}{B_0} , \tag{28}$$

where $\tau_c(t)$ is the synchrotron plus inverse Compton cooling time,

$$\tau_c = 3P_0/L_{s c 0} , \tag{29}$$

V_S is the sound speed

$$V_S = (4P_0/3\rho_0)^{1/2} , \tag{30}$$

$$\bar{k} = k\left(1 + \frac{\tan kr}{kr}\right) , \tag{31}$$

$k(t) = 2\pi/\lambda(t)$, and from equation (13) in the linear approximation

$$\lambda(t) = \alpha_\lambda R(t) , \tag{32}$$

where α_λ is a given constant fraction of the radius R.

The coefficients of the first-order equations are not constant. Consequently, we cannot solve the system in the steady state case, as in previous works. We must instead solve the linearized equations numerically. In the short-wavelength limit, however, when the condition

$$\tau_{AS} \equiv \frac{\lambda}{2\pi(V_A^2 + V_S^2)^{1/2}} < \tau_c \tag{33}$$

is satisfied, we can obtain an analytic solution of equations (25)–(28). In equation (33), V_A is the Alfvén velocity ($V_A^2 = B_0^2/4\pi\rho_0$) and τ_{AS} is the time it takes for a magnetosonic wave to cross the perturbed region. When we have equation (33), the pressure in the perturbed region is equalized in a time small compared with the cooling time τ_c. The condensation is then increasing under constant pressure. From $P + (B^2/8\pi) = $ constant, we have

$$\hat{P}_1 + \frac{B_0}{4\pi}\hat{B}_1 = 0 . \tag{34}$$

If this isobaric condition is combined with equations (25)–(28), we obtain

$$\frac{\hat{\rho}_1(t)}{\hat{\rho}_1(0)} = \exp\left\{\int_0^t \frac{q[-(2/3)\nu_e - (2/\tau_c)] + 3(2\eta_0 - 1)/4\tau_c - 2\nu_e}{q + 1} dt\right\} , \tag{35}$$

where, again, $q = V_A^2/V_S^2$.

From equation (35), the condition to have an instability is

$$q < \frac{-2\nu_e + 3(2\eta_0 - 1)/(4\tau_c)}{(2/3)\nu_e + 2/\tau_c} . \tag{36}$$

For the general case, for an arbitrary λ, equations (25)–(28) must be solved numerically.

When the expansion rate is zero (i.e., $\nu_e = 0$), we have from equation (36) the condition $q < (3/8)(2\eta_0 - 1)$, which is the condition for the thermal instability obtained by Simon and Axford (1967).

As expected, the condensation grows faster in the absence of expansion. We note also that in the absence of both inverse Compton scattering ($\eta_0 = 1$) and expansion ($\nu_e = 0$), equation (36) gives $q < 3/8$.

From equation (36), the fact that q is a real and positive quantity puts an upper limit on τ_c in order to have a thermal instability.

$$\tau_c < (3/8)(2\eta_0 - 1)/\nu_e . \tag{37}$$

Equation (35) shows that in the absence of inverse Compton losses ($\eta_0 = 1$) the condensation grows faster than when they are present ($\eta_0 < 1$), thus confirming the conclusion of previous authors (e.g., Eilek and Caroff 1979) that inverse Compton losses tend to stabilize the system.

We see that the instability criterion (eq. [37]), in the presence of inverse Compton losses ($\eta_0 < 1$), restricts more the range of values of τ_c for which we have growth of the thermal instability.

We found that the most unstable disturbances (i.e., maximum growth) are those with wavelengths λ less than $\lambda_c \cong (v_A^2 + v_s^2)^{1/2}\tau_c$, which, according to equation (33), is the critical λ under which the disturbances grow under isobaric conditions. For $\lambda > \lambda_c$ (i.e. out

of pressure equilibrium) accelerations acting against collapse may develop in the perturbed region, inhibiting the amplification of the perturbed density.

V. NONLINEAR EQUATIONS

Because the linearized equations are valid only when the perturbations are small compared with the zeroth-order quantities, we are not able to deduce the true density enhancements from the linear analysis. A nonlinear treatment is required for that. Thus, if we drop the condition that the perturbed quantities are small compared with the unperturbed ones, keeping all higher order terms, we have the following set of equations for the perturbed quantities:

$$\dot{\hat{\rho}}_1(t) = \hat{\rho}_1[\dot{k}r \tan(kr) + kr \tan(kr)v_e - 2v_e] + [\sin(kr)\tan(kr)k - \bar{k}\cos(kr)]\hat{v}_1\hat{\rho}_1 - \rho_0\bar{k}\hat{v}_1 , \quad (38)$$

$$\dot{\hat{B}}_1(t) = \hat{B}_1[\dot{k}r \tan(kr) + kr \tan(kr)v_e - 2v_e] + [\sin(kr)\tan(kr)k - \bar{k}\cos(kr)]\hat{v}_1\hat{B}_1 - B_0\bar{k}\hat{v}_1 , \quad (39)$$

$$\dot{\hat{P}}_1(t) = \hat{P}_1[\dot{k}r \tan(kr) + kr \tan(kr)v_e - 2v_e] + [\sin(kr)\tan(kr)k - \Gamma\bar{k}\cos(kr)]\hat{v}_1\hat{P}_1 - \Gamma P_0\bar{k}\hat{v}_1 - (\Gamma - 1)\frac{(L_{s1} + L_{c1})}{\cos(kr)} , \quad (40)$$

$$\dot{\hat{v}}_1(t) = -\hat{v}_1\left[\frac{\dot{k}r}{\tan(kr)} + v_e\frac{kr}{\tan(kr)} + v_e\right] - \cos(kr)k\hat{v}_1^2 + \frac{k}{\rho_0 + \hat{\rho}_1\cos(kr)}\left[\hat{P}_1 + \frac{B_0}{4\pi}\hat{B}_1 + \frac{\hat{B}_1^2}{4\pi}\cos(kr)\right] . \quad (41)$$

The change of the synchrotron losses in the perturbed region is

$$L_{s1}(r, t) = L_{s0}\left\{\left[\frac{\hat{P}_1}{P_0}\cos(kr) + 1\right]^2\left[1 + \frac{\hat{\rho}_1}{\rho_0}\cos(kr)\right]^{-1}\left[1 + \frac{\hat{B}_1}{B_0}\cos(kr)\right]^2 - 1\right\} , \quad (42)$$

and the change of the inverse Compton losses is

$$L_{c1}(r, t) = L_{c0}\left\{\left[\frac{\hat{P}_1}{P_0}\cos(kr) + 1\right]^2\left[1 + \frac{\hat{\rho}_1}{\rho_0}\cos(kr)\right]^{-1} - 1\right\} , \quad (43)$$

where L_{c0} is the inverse Compton loss function of the ambient medium $L_{c0} = (1 - \eta_0)L_{sc0}$.

In equations (38)–(41), $k(t)$ is determined by the condition of the conservation of magnetic flux in the perturbed region (eq. [13]),

$$k(t) = \frac{2\pi}{\alpha_B}\left\{\frac{\hat{B}_1(t)}{2\pi}\left(\frac{\pi}{2} - 1\right) + \frac{\pi}{16}B_0(0)\left[\frac{R(0)}{R(t)}\right]^2\right\}^{1/2} , \quad (44)$$

where α_B is a constant that depends on the initial values of $\hat{B}_1(0)$ and $k(0)$:

$$\alpha_B = \frac{2\pi}{k(0)}\left[\hat{B}_1(0)\left(\frac{1}{4} - \frac{1}{2\pi}\right) + \frac{\pi}{16}B_0(0)\right]^{1/2} . \quad (45)$$

In the limit $\hat{B}_1(0) \ll B_0(0)$ (linear approximation), equation (44) reduces to the linear dependence $k(t) \propto R(t)^{-1}$ (eq. [32]). Similarly, equations (38)–(41) reduce to equations (25)–(28) when the linear approximation is made.

VI. RESULTS

We applied the above equations to the inner radio jet in Cen A and the radio lobe Cyg A.

a) Cen A

The radio emission from Cen A contains many scale sizes of structure (Burns, Feigelson, and Schreier 1983). Recent very high resolution VLA data at 2 and 6 cm (Clarke, Burns, and Feigelson 1986) showed that the inner 40″ of the jet of Cen A is far more complex than previously perceived. While knot A appeared to be a simple circular structure at 10″ resolution and a string of circular knots (designated A1, A2, A3, and A4 knots) at 1″ resolution (Burns, Feigelson, and Schreier 1983), at 0″.3 resolution it is found to be a complex combination of subknots and filamentary structure which the authors call "streamers." Streamers with a typical radius ~20 pc were observed which corresponds to 30% of the radius of knot A1 at 1″ resolution. In order to investigate the possibility that the filamentary structure is due to a thermal instability, we used the above equations with the following initial conditions.

We assumed initially $\dot{\hat{\rho}}_1(0) = 0$ and the isobaric condition (eqs. [35] and [36]) which implies

$$q(0) = \frac{-2v_e + (3/4\tau_c)(2\eta_0 - 1)}{(2/3)v_e + (2/\tau_c)} . \quad (46)$$

We used as initial values for the parameters of the jet (extracted from the observational data): $R(0) = 2 \times 10^{20}$ cm (radius of the jet in the region of the A1 knot), $\theta = 6°$, and $P_0(0) = 10^{-10}$ dynes cm^{-2} (estimated from minimum energy considerations; Burns, Feigelson, and Schreier 1983). We also assumed for the jet a velocity of $V_J = 5000$ km s^{-1}. This value, based primarily on energy requirements, was the best estimate for V_J obtained by Burns, Feigelson, and Schreier (1983) after considering six different model-dependent assumptions (a freely expanding jet model, relativistic beaming, synchrotron lifetime arguments, energy considerations, dynamical bending or kinking of the jet, and helical instabilities). For the initial ambient thermal density we adopted the value $\rho_0(0) = 10^{-26}$ g cm^{-3} which, according to Burns, Feigelson, and Schreier (1983), is a best guess from polarization arguments. These initial values, and equation (46), imply $B_0(0) = 2.14 \times 10^{-5}$ G and an initial ratio of the pressure of the relativistic electrons to the magnetic pressure $\beta(0) = P_0(0)/P_{M0}(0) = 5.49$. The redshift used for Cen A was $Z = 0.0012$ (Bridle and Perley 1984).

We note that, owing to the assumption of initial marginal stability of equation (46), the ratio $P_0(0)/P_{Mo}(0)$ is greater than the equipartition value $(P_0/P_{Mo})_{eq} \cong 4/3$ (Burns, Owen, and Rudnick 1979). We may expect that the equipartitioning of the energy between the electrons and the magnetic field requires special conditions, such as the presence of some turbulence. A particularly intense luminous region, such as the A1 knot in the Cen A jet, may be such a region. When the special conditions cease to exist, and the magnetic field decreases due to the expansion of the jet, the ratio P_0/P_{Mo} rapidly increases from the equipartition value 4/3 to the marginal stability value given by equation (46).

The synchrotron plus inverse Compton loss function, L_{sco}, is determined from observations, i.e., from the observed luminosity and inferred volume of the source. Therefore, its determination for each source depends on the available data. In the case of the inner jet of Cen A, we have information on the observed luminosity in the radio to X-ray range for different regions of the source, and L_{sco} was determined from the integrated observed luminosity from radio to X-rays. Calculations considering only the radio contribution for L_{sco} in Cen A revealed no appreciable increase of the rate of condensation. However, the integrated luminosity from radio to X-rays cannot be determined for most sources because of the lack of data (in particular, in the X-ray and visible regions). This is the case of the Cyg A source, for which we have assumed L_{sco} to be given only by the *radio* luminosity per unit volume, as discussed later in this section.

The variation of L_{sco} with time was assumed in the calculations for the inner Cen A jet to have the following linear form

$$L_{sco}(t) = L_{sco}(0)\left[1 + \frac{\alpha_{sc} t V_J}{R(0)} \right], \qquad (47)$$

where α_{sc} is a constant.

The two values $L_{sco}(0)$ and α_{sc} were determined from the radiation losses in the regions A1 and B of the Cen A jet. The loss function L_{sc} (A1) and L_{sc} (B) were obtained from the integrated observed luminosity from X-rays to radio, using the radio-optical data of Burns, Feigelson, and Schreier (1983) and the X-ray data of Feigelson *et al.* (1981). According to Burns, Feigelson, and Schreier (1983), the observed spectra between radio and X-rays is consistent with a power-law model with a "break" at optical wavelengths. The radio spectral indices between 6 and 20 cm are $\alpha_6^{20}(A1) = 0.5$ and $\alpha_6^{20}(B) = 0.7$, and the indices between 6 cm and 2 keV are $\alpha_X^6(A1) = 0.83$ and $\alpha_X^6(B) = 0.78$. The resultant spectrum implies a "break" at optical wavelengths, similar to that observed in M87 (Stocke, Rieke, and Lebofsky 1981; Schreier, Gorenstein, and Feigelson 1982) at $\nu \sim 6 \times 10^{14}$ Hz. The losses $L_{sc}(A1)$ and $L_{sc}(B)$ [from which we obtain $L_{sco}(0)$ and α_{sc}] were evaluated assuming: (1) with Brodie, Königl, and Bowyer (1983) that the radio to X-ray spectra has a break at $\nu \sim 6 \times 10^{14}$ Hz; (2) the observed spectral indices α_6^{20} and α_X^6; (3) a low-frequency cutoff at $\nu \sim 10^7$ Hz; (4) a high-frequency cutoff at $\nu \sim 5 \times 10^{17}$ Hz (2 keV); and (5) emission volumes inferred from the radio observation of Brodie, Königl, and Bowyer (1983). The resultant values for $L_{sco}(0)$ and α_{sc} used in equation (47) were $L_{sco}(0) = 10^{-21}$ ergs cm^{-3} s^{-1} and $\alpha_{sc} \cong -0.05$.

Equation (47) is a very crude approximation to the observational data. However, we found that an exponential fit for equation (47) produced essentially the same results for the emissivity contrasts shown below.

The nonlinear calculations were first tested with an initial small perturbation $\hat{\rho}_1(0)/\rho_0(0) = 10^{-5}$ in order to check agreement with the results of the linearized theory; agreement of better than 5% was verified (including inverse Compton losses) for a time scale of $t = 26.6\tau_c(0)$.

Equations (38)–(41) were integrated at a fixed radius r of the density profile described by the cosine distribution (eq. [11]), but with $k(t)$ varying according to equation (44). In general, we used an initial $\lambda(0) = 0.1R(0)$ and chose the middle of the adopted cosine profile $k(0)r = \pi/4$ for the beginning of the calculations.

The nonlinear evolution of the density perturbation $\hat{\rho}_1(t)/\hat{\rho}_1(0)$, with initial density perturbations $\alpha_\rho = \hat{\rho}_1(0)/\rho_0(0) = 0.05, 0.1, 0.2$, and 0.3 are shown in Figure 1. In the time interval of integration considered in Figure 1, which corresponds approximately to the distance $(= V_J \Delta t$ with $V_J \cong 5000$ km^{-1} s^{-1}) between the knots A1 and B of the Cen A jet (where the bright filaments were observed), we find that the nonlinear evolution, for example, for $\hat{\rho}_1(0)/\rho_0(0) = 0.1$, reaches a maximum at a time $t_{max} \cong 1.3 \times 10^5$ yr. This time can be compared with the cooling time $\tau_c(0) = 3P_0/L_{sco}(0) = 9.5 \times 10^3$ yr [i.e., $t_{max} \cong 13.7\tau_c(0)$].

There is a slight dependence of the beginning of the maximum with α_ρ: for an increasing initial perturbation (α_ρ), the maximum is attained slightly earlier.

The calculations with an initial perturbation 2 and 3 times as large $(\alpha_\rho = 0.2$ and 0.3, respectively) and also one half as large $(\alpha_\rho = 0.05)$ as the perturbation $\alpha_\rho = 0.1$, were found to produce approximately the same density contrast ρ_p/ρ_0, as can be seen in Figure 2. For example, at the time 1.5×10^5 yr, the density contrast of the perturbed region ρ_p/ρ_0 for the initial perturbations $\alpha_\rho = 0.05, 0.1, 0.2$, and 0.3 is $\rho_p/\rho_0 \cong 6.5$ and at $t \cong 2.0 \times 10^5$ yr $\rho_p/\rho_0 = 8.4$.

It is interesting to note that, although the different initial perturbations reach the same maximum density contrast at the time $t \sim 2.0 \times 10^5$ yr, at earlier time the growth of ρ_p/ρ_0 (Fig. 2) for smaller values of α_ρ is slower. We note also that, although the perturbed quantity $\hat{\rho}_1(t)/\hat{\rho}_1(0)$ (Fig. 1) decreases after a certain time, the density contrast ρ_p/ρ_0 continues to increase because of the decrease of the ambient density with the jet expansion. Calculations with smaller values of α_ρ ($10^{-5} \leq \alpha_\rho \leq 10^{-2}$) were also made, and we found that for $\alpha_\rho \leq 10^{-2}$ the curves fall in the linear regime.

Figure 3 shows for the different values of α_ρ of Figures 1 and 2 the ratios of the electronic pressure (of the condensed region) (P_p) to the ambient electronic pressure (P_0).

Figure 4 compares the electronic pressure (P_p), the magnetic pressure (P_{Mp}) and the total pressure $(P_{tot_p} = P_p + P_{Mp})$ of the perturbed region for $\alpha_\rho = 0.1$. (Similar behavior was also found for the other values of α_ρ.) The ambient electronic pressure P_0 (given by eq. [24]) is also given in Fig. 4. We note that the electronic pressure (P_p) is dominant over the magnetic pressure (P_{Mp}), except at the end of the time interval.

Comparing Figures 1–4, we note that the decrease of $\hat{\rho}_1(t)/\hat{\rho}_1(0)$ after attaining the maximum value is coincident with the decreasing difference between P_p and P_{Mp}.
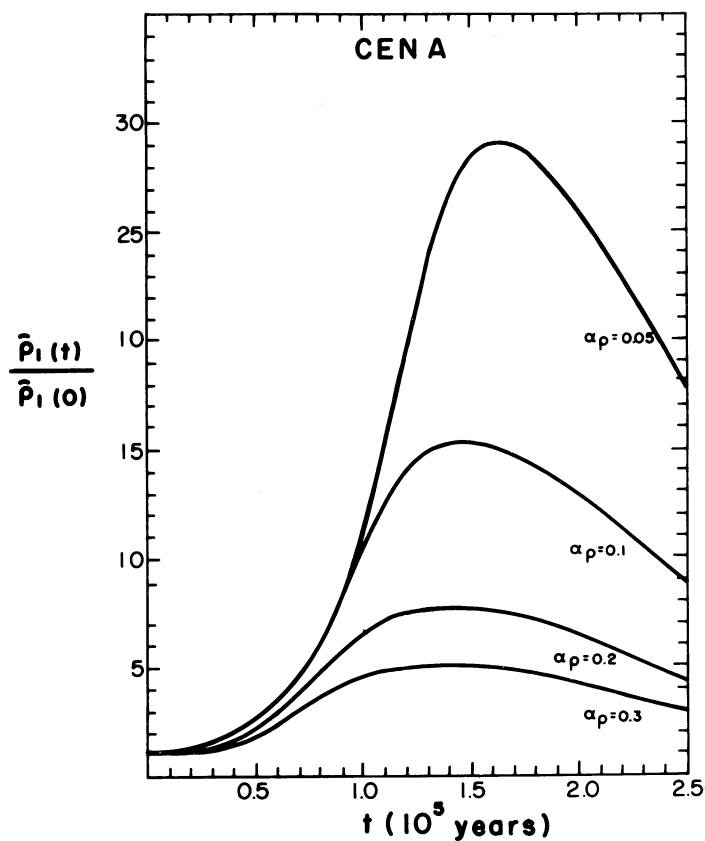
FIG. 1.—Nonlinear growth curves of $\hat{\rho}_1(t)/\hat{\rho}_1(0)$ in the inner jet of Cen A for initial density perturbations $\alpha_\rho[\equiv \hat{\rho}_1(0)/\rho_0(0)] = 0.05, 0.1, 0.2,$ and 0.3
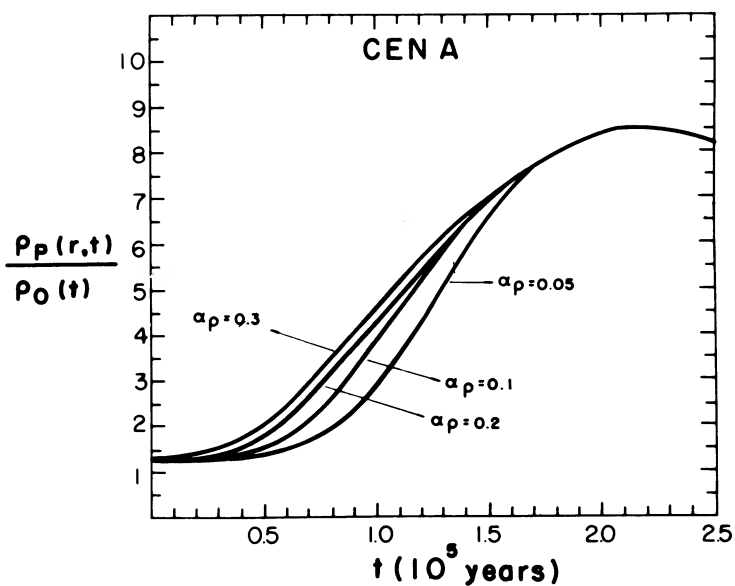
FIG. 2.—Nonlinear growth curves of the total density contrast of the perturbed region ρ_p/ρ_0 in the inner jet of Cen A for initial density perturbations $\alpha_\rho[\equiv \hat{\rho}_1(0)/\rho_0(0)] = 0.05, 0.1, 0.2,$ and 0.3.
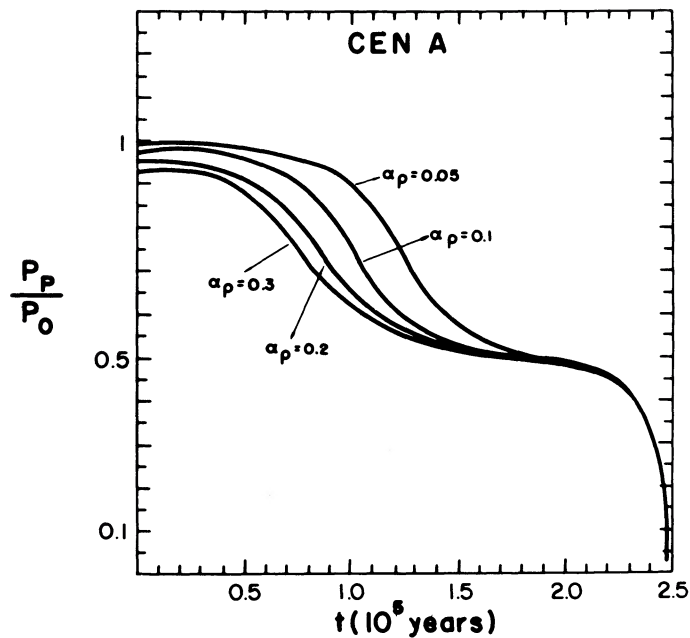
FIG. 3.—The ratio of the electronic pressure of the condensed region, P_p, to the ambient electronic pressure, P_0, in the inner jet of Cen A, for initial density perturbations $\alpha_\rho[\equiv \hat{\rho}_1(0)/\rho_0(0)] = 0.05, 0.1, 0.2$, and 0.3.
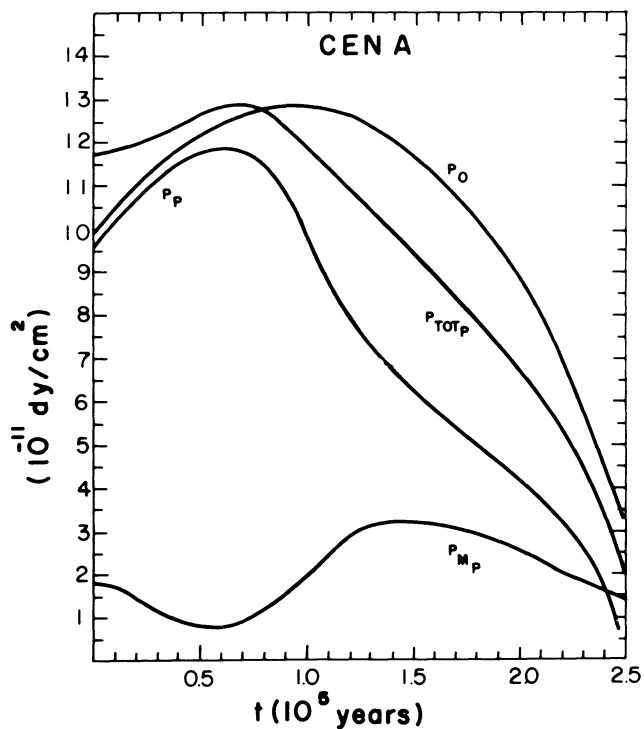
FIG. 4.—Comparison of the electronic pressure (P_p), the magnetic pressure (P_{Mp}) and the total pressure (P_{tot_p}) of the perturbed region in the inner jet of Cen A for $\alpha_\rho = 0.1$.

The nonlinear evolution of the condensation curve as shown in Figures 1 and 2 can be understood as follows. The thermal instability develops when we have $q \leq q_0 < q_{eq}$. This implies the dominance of the electron pressure over the magnetic pressure in the ambient region. In the region of the perturbation, the electron pressure is less than the ambient pressure, causing a compression of the perturbed region. This compression involves an increase in the magnetic field of the perturbed region, and an increase of the magnetic pressure. When the magnetic pressure in the perturbed region becomes comparable to the difference in the electron pressures of the ambient and perturbed regions, no further condensation occurs. Comparing the curves of Figures 2–4 we note that the maximum of the condensation is attained for approximately isobaric conditions. The electronic pressure ratio P_p/P_0 varies from ~ 1 to ~ 0.5 in the time interval $\Delta t \sim 2.2 \times 10^5$ yr, and the total pressure ratio P_{tot_p}/P_{tot_0} varies from 1 to ~ 0.77 in the same time interval (where P_{tot_0} is the total pressure of the ambient region).

At $t = 0$ we have $P_0 = 1.0 \times 10^{-10}$ dynes cm^{-2} and $q = 0.27$ (which can be compared with the values, for example, of $q \cong 10^{-3}$ and $q \cong 0$ studied by Marscher 1980). At the time of the maximum $\hat{\rho}_1(t)/\rho_1(0)$ ($t \cong 1.3 \times 10^6$ yr) in Figure 1 for $\alpha_\rho = 0.1$, for example, we have $\rho_p/\rho_0 = 5.9$, $P_p/P_0 = 0.57$, and a small increase of pressure $P_0 \cong 1.24 \times 10^{-10}$ dynes cm^{-2}. As we saw earlier, equation (7) gives the ratio of the synchrotron energy losses (in ergs s^{-1} cm^{-3}) in the perturbed region (L_{sp}) to the adjacent ambient region $(\bar{L}_{s0})$. For $\alpha_\rho = 0.1$, for example, at $t \cong 1.3 \times 10^6$ yr, we found according to equation (7) for $F = 0.5$, $L_{sp}/\bar{L}_{s0} = 3.5$ and for $F = 0.1$, $L_{sp}/\bar{L}_{s0} = 16.2$; at the time $t \cong 0.8 \times 10^5$ yr, for which $\rho_p/\rho_0 = 2.14$ and $P_p/P_0 \cong 0.90$, we have $L_{sp}/\bar{L}_{s0} = 2.7$–10 (for $F = 0.5$–0.1); and at the time $t \cong 2.1 \times 10^5$ yr, for which $\rho_p/\rho_0 = 8.4$ and $P_p/P_0 \cong 0.48$, we have $L_{sp}/\bar{L}_{s0} = 3.6$–17.2 ($F = 0.5$–0.1). These values show that the synchrotron energy loss contrast is only slightly dependent on t.

We note that the distances corresponding to the time intervals above $(V_J t)$ are poorly defined due to the great uncertainty of V_J; it is difficult to specify the exact distance which corresponds to the time, for example, of $t \sim 0.8 \times 10^5$ yr. We note, however, using acceptable values of V_J, we obtain distances comparable to the distance between knot A1 and knot A4 where data reveal the filamentary structure called "streamers" (Clarke, Burns, and Feigelson 1986).

In order to compare the above calculated results $L_{sp}/\bar{L}_{s0} \cong 2.7$–17.2 with observations, we proceeded as follows. To obtain the energy losses of the perturbed region (L_{sp}) from observations, we used the data on the radio filaments or "streamers" observed in the inner Cen A jet at high resolution by Clarke, Burns, and Feigelson (1986). To estimate the rate of energy losses in the ambient region, we used the radio data obtained at a lower resolution for the inner Cen A knots by Burns, Feigelson, and Schreier (1983). From the observed surface brightness and spectral index, in both cases, we estimated the corresponding radio luminosities (in ergs s^{-1}), and, using the inferred volume of the features given by the authors, we obtained the corresponding radio volume emissivities (in ergs cm^{-3} s^{-1}) for the filaments and adjacent regions. Assuming that the ratio of the *radio* energy losses (or radio volume emissivities) between the perturbed and ambient regions is synchrotronic, we obtain $L_{sp}/\bar{L}_{s0} \cong 4$–8, in reasonable agreement with our calculated results $L_{sp}/\bar{L}_{s0} \cong 2.7$–17.2 for $0.1 \lesssim F \lesssim 0.5$. These results indicate that the thermal instability appears to be sufficient to explain the filaments in the inner jet of Cen A observed by Clarke, Burns, and Feigelson (1986). We note, however, that there is a great uncertainty in the value of $L_{sp}/\bar{L}_{s0}$ inferred from the observations.

As mentioned earlier, the exponential fit, for equation (47) produces essentially the same contrasts for the above synchrotron radio emissivity. We found that an exponential fit gives a lower density amplification which is compensated by a larger ratio P_p/P_0 giving values of $L_{sp}/\bar{L}_{s0}$ very similar to those found above.

As was noted previously, in the above calculations, we assumed initial marginal stability (eq. [46]). If we start our calculations from the equipartition condition $[P_0(0)/P_{M0}(0) \cong 4/3]$ at the position of the A1 knot, our results show that the position of marginal stability (assuming $\alpha_\rho = 0.1$) is attained in a time $t \sim 1.7 \times 10^5$ yr, and at a time $t \cong 2.1 \times 10^5$ yr the corresponding density contrast is $\rho_p/\rho_0 = 2.0$ and $P_p/P_0 = 0.95$. These values can be compared with $\rho_p/\rho_0 = 8.4$ and $P_p/P_0 = 0.48$ found for $\beta(0) = 5.5$ (see Figs. 2 and 3) at the same time. These values show that although we have a decrease of the density contrast ρ_p/ρ_0 under equipartition conditions, the ratio P_p/P_0, on the other hand, increases when compared to the ratio for $\beta(0) = 5.5$, implying a synchrotron energy loss contrast $L_{sp}/\bar{L}_{s0} \cong 2.7$ (for $F = 0.5$), in fairly good agreement with the value of $L_{sp}/\bar{L}_{s0}$ obtained for $\beta(0) = 5.5$ at $t \cong 2.1 \times 10^5$ yr $(L_{sp}/\bar{L}_{s0} \cong 3.6)$.

It is interesting to note that although in the linear region inverse Compton losses strongly suppress the growth of the thermal instability, they do not decrease the nonlinear density contrast appreciably.

For example, for times $t \gtrsim 1.5 \times 10^5$ yr, the difference in the linear curves of $\hat{\rho}_1(t)/\hat{\rho}_1(0)$ with and without inverse Compton losses is $\gtrsim 50\%$, while for an initial perturbation $\alpha_\rho = \hat{\rho}_1(0)/\rho_0(0) = 0.1$ the difference in the nonlinear curves with and without inverse Compton losses is less than 30%. The low sensitivity of these nonlinear results to the IC losses is due to the high initial magnetic and electronic pressures compared with the IC equivalent pressure $B_{CI}^2/8\pi \equiv P_{CI}$. In the curves of Figures 1–4 we have the ratio $\beta(0) = P_0(0)/P_{M0}(0) = 5.49$ and $\delta(0) = P_{CI}/P_{M0} = 0.022$.

In order to check the sensitivity of our nonlinear results to the IC losses, we performed calculations with other (probably unrealistic) values of the ratio $\delta(0)$ to increase artificially the IC losses. Figure 5 shows the evolution ρ_p/ρ_0 for different values of $\delta(0) = P_{CI}/P_{M0}$. All curves have an initial perturbation $\alpha_\rho = 0.1$ with the other initial conditions the same as in the other figures with $\beta(0) = 5.49$. For comparison, we have again plotted the curve with $\alpha_\rho = 0.1$ and $\delta(0) = 0.022$ of Figure 2. We found that in the range $0.05 \lesssim \delta(0) < 0.10$, the curves were approximately the same as for $\delta(0) = 0.10$. We found that as we increase $\delta(0)$ from $\delta(0) = 0.022$ to $\delta(0) < 0.14$ leaving $\beta(0)$ unaltered, we still have a density amplification. We note, however, that when $\delta(0) \geq 0.14$, there is a strong suppression of the instability. The curve with $\delta(0) = 0.14$ can be compared with the curve with $\delta(0) = 0.022$ (which has the parameters appropriate for the Cen A jet). These results show that only for conditions very different from those that are expected to occur in this source would IC losses suppress the growth of condensations.

The decrease of ρ_p/ρ_0 by increasing $\delta(0)$ is accompanied by a slower decrease of P_p/P_0 in Figure 3. For example, while for $\delta(0) = 0$ at $t \cong 2 \times 10^5$ yr we have $\rho_p/\rho_0 = 11$ and $P_p/P_0 = 0.34$, for $\delta(0) = 0.022$, at $t \cong 2 \times 10^5$ yr we have $\rho_p/\rho_0 = 8.2$ and $P_p/P_0 = 0.48$, and for $\delta(0) = 0.1$ we have $\rho_p/\rho_0 = 5.7$ and $P_p/P_0 = 0.71$. These values and equation (7) imply, for $F = 0.5$, $L_{sp}/\bar{L}_{s0} \cong 2.4$ for $\delta(0) = 0$, $L_{sp}/\bar{L}_{s0} = 3.6$ for $\delta(0) = 0.022$, and $L_{sp}/\bar{L}_{s0} \cong 5.2$ for $\delta(0) = 0.1$.
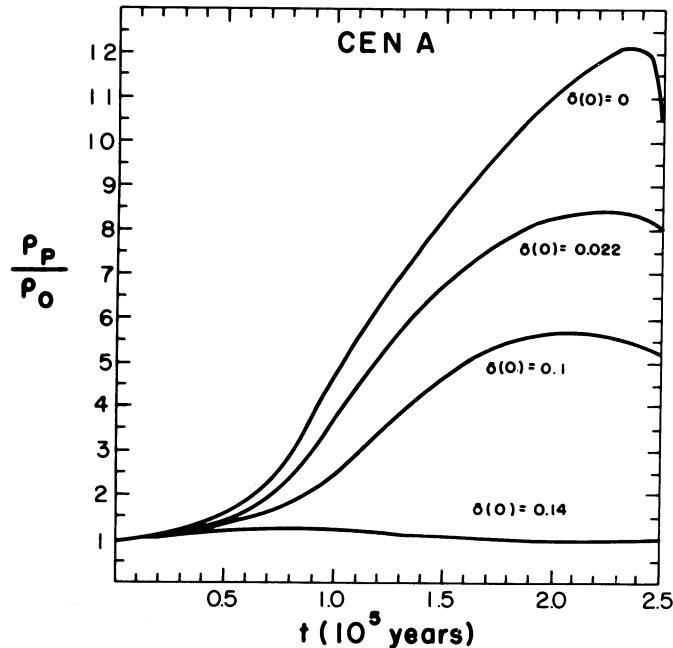
FIG. 5.—Nonlinear growth curves of the total density contrast $\rho_p/\rho_0 (\equiv [\rho_1(r, t) + \rho_0(t)/\rho_0(t)])$ in the inner jet of Cen A for $\alpha_p = 0.1$ and initial ratios of the magnetic pressure to the equivalent inverse Compton pressure $\delta(0)[\equiv P_{CI}/P_{Mo}(0)] = 0.022, 0.10$, and 0.14.

We thus see that, although the increase in the IC losses inhibit the growth of the condensations, the increase of P_p/P_0, on the other hand, creates a good energy loss contrast, and for $\delta(0) \lesssim 0.1$, $L_{sp}/\bar{L}_{s0}$ is relatively insensitive to the presence of IC losses.

As noted previously, we used in the calculations, in general, an initial value $\lambda(0) = 0.1R(0)$. Nonlinear calculations with smaller and greater values of $\lambda(0)$ [i.e. $\lambda(0) = 0.01, 0.05, 0.2, 0.3$, and $0.4R(0)$] were also performed and produced the same results as the curves with $\lambda(0) = 0.1R(0)$ shown in the above figures.

In the linear regime, there is no difference in the results obtained for any initial $k(0)r$. In the nonlinear regime, however, there is a slight dependence on $k(0)r$. The middle of the cosine profile, $k(0)r = 45°$, was chosen because it describes a reasonable approximate average change of density with radius expected for the perturbed region. Calculations with $k(0)r = 10°, 30°$, and $60°$ were also made, and similar density amplifications were obtained. At the time when ρ_p/ρ_0 reaches a maximum, an agreement of $\sim 1\%$ was found. Since the pressure gradient profile, which represents the force acting on the surface of the perturbed region or filament, depends on $\nabla_r[\cos^2 k(t)r]$ through $B_1^2/8\pi$ and depends on $\nabla_r[\cos k(t)r]$ through P_1 and $B_1B_0/4\pi$, the force on the surface increases with increasing phase angle. Larger angles (e.g., $>60°$) give larger than expected gradients and smaller angles (e.g., $<10°$) give smaller than expected gradients. The use of $k(0)r = 45°$ is an approximation, however; multidimensional calculations in the future should give more detailed information on the space time development of the thermal instability.

The numerical calculations shown in Figures 1–5 were performed with $V_J = 5000$ km s^{-1}. The recent analysis of Clarke, Burns, and Feigelson (1986) implies a $V_J \sim 2.3$ times this value $(= 1.15 \times 10^4$ km s$^{-1})$. We found for this new value of V_J that because we have an increase in the expansion rate $v_e(t)$ of ~ 2.3 times greater (suggesting a possible suppression of the thermal instability from eq. [37]) the density contrast is lower. For example, for $\alpha_p = 0.1$, we found that at $t \cong 0.9 \times 10^5$ yr (which corresponds to a distance from the A1 knot $V_J t \cong 3.3 \times 10^{21}$ cm) ρ_p/ρ_0 attains a maximum value $\rho_p/\rho_0 = 1.9$ which is one-fourth the value found in Figure 2 at the same distance (i.e., $\rho_p/\rho_0 = 8.4$ at a distance $V_J t = 3.3 \times 10^{21}$ cm and $t = 2.1 \times 10^6$ yr). The corresponding value of P_p/P_0, on the other hand, is larger; while for $V_J = 5000$ km s^{-1} we found $P_p/P_0 = 0.48$ at $V_J t = 3.3 \times 10^{21}$ cm, for $V_J = 1.15 \times 10^4$ km s^{-1} we found $P_p/P_0 = 0.99$. These values and equation (7) imply $L_{sp}/\bar{L}_{s0} \cong 2.7–9.8$, for $F = 0.5–0.1$, and $V_J = 1.15 \times 10^4$ km s^{-1} (which is in good agreement with the estimated values for $V_J = 5000$ km s^{-1}).

b) Cyg A

The radio lobe of Cyg A shows a rich filamentary structure (Perley, Dreher, and Cowan 1984), more or less aligned with the axis of the radio source, in the region of the lobe close to the nucleus, and more amorphous in the extremities of the lobes where are found the hot spots. In order to obtain the appropriate initial parameters, we consider the region of the source where the jet enters the lobe. In this region, we assume a slowing down of the jet, and a velocity V_J on the order of the expansion velocity of the lobe in the ambient medium. On the assumption that the axis of Cyg A lies in the plane of the sky, and assuming for the total age of the source 6×10^6 yr, Winter et al. (1980) estimated a mean expansion speed of $0.05c$. This value is similar to the speed of $0.04c$ derived by Hargrave and Ryle (1974) assuming a value for the density of the intergalactic medium and ram pressure balance at the hot spots in Cyg A. Another recent estimate of the expansion velocity of the lobe into the external medium by Dreher et al. (1987) gives $V_J = 0.1c$. In the present calculation we assumed for V_J, when the jet enters the lobe, the range of values $V_J \cong 0.01–0.1c$. For the mass density of the jet material which enters the lobe, we assumed $\rho_0(0) = 1.7 \times 10^{-29}$ g cm^{-3} [or $n_{tot_0}(0) = 10^{-5}$ cm^{-3}]. This value was estimated by Perley, Dreher, and Cowan (1984) as an upper limit for the Cyg A jet. The initial values of the other parameters,

estimated from the synchrotron observations are (Hargrave and Ryle 1974; Perley, Dreher, and Cowan 1984; Dreher et al. 1986): $R(0) = 5 \times 10^{21}$ cm (the radius of the jet when it enters the lobe, assuming a jet opening angle of $2°5$ and jet extension of ~ 40 kpc; Dreher 1985), $\theta = 2°5$, $P_0(0) = 5 \times 10^{-11}$ dynes cm^{-2} (the gas pressure in the interfilament medium; Perley, Dreher, and Cowan 1984), and $L_{sco} = 10^{-23}$ ergs cm^{-3} s^{-1} (assumed to be consistent with distance along the jet in the lobe) (obtained by considering a mean radio luminosity of 10^{45} ergs s^{-1} and source volume $\sim 10^{68}$ cm^3; (Perley, Dreher, and Cowan 1984). In order to evaluate the energy losses due to inverse Compton losses, a redshift $Z = 0.057$ was used (Bridle and Perley 1984). The corresponding initial cooling time is $\tau_c = 3P_0/L_{sco} = 5 \times 10^5$ yr.

As in the analysis of Cen A, we assume as an initial condition $\dot{\rho}_1(0) = 0$. This condition, implying equation (46), gives $B_0(0) = 1.6 \times 10^{-5}$ G and $\beta(0) = 5.09$ for $V_J = 0.01c$.

Nonlinear calculations for Cyg A, using $\hat{\rho}_1(0)/\rho_0(0) = 0.1$, $k(0)r \cong \pi/4$, and velocities $V_J = 0.01c, 0.033c, 0.05c$, and $0.1c$ were made, and the evolution of the density contrast ρ_p/ρ_0 as a function of the distance ($z = V_J t$) from the origin of the integration is shown in Figure 6 for $V_J = 0.01c, 0.033c$, and $0.05c$. We observe, for example, that for $V_J = 0.01c$ the maximum of $\rho_p/\rho_0 = 4.8$ occurs at a distance $z = 1 \times 10^{23}$ cm corresponding to a time $t(=z/V_J) \cong 1 \times 10^7$ yr and at $z \cong 6.3 \times 10^{22}$ cm ($t \cong 6.6 \times 10^6$ yr) $\rho_p/\rho_0 = 2.9$. For $V_J = 0.033c$, a maximum of $\rho_p/\rho_0 = 2$ is attained at a distance 1.6×10^{23} cm, corresponding to $t \cong 5.1 \times 10^6$ yr. These times can be compared with the estimated age of Cyg A $\sim 6 \times 10^6$ yr (Hargrave and Ryle 1974; Pelletier and Roland 1986). Similarly, the above distances can be compared with the estimated extension of the lobes of Cyg A of ~ 33 kpc $\cong 1.02 \times 10^{23}$ cm (obtained assuming $H_0 = 50$ km s^{-1} Mpc and $Z = 0.056$, Hargrave and Ryle 1974) and the typical extension of the observed filaments $\lesssim 20$ kpc $\cong 6.2 \times 10^{22}$ cm (Perley, Dreher, and Cowan 1984).

We see that when V_J is increased, the maximum density contrast is reached at larger distances and earlier times ($t = \Delta z/V_J$) and with smaller values of ρ_p/ρ_0. We saw earlier that the reason for this decrease with V_J in the density contrast is that we have an increase of the expansion rate relative to the cooling rate. Figure 6 shows that for larger values of $V_J \gtrsim 0.05c$ the expansion rate will cause the suppression of the thermal instability. We see that for $V_J = 0.05c$ the maximum value of $\rho_p/\rho_0 < 1.5$.

Figure 7 shows, for $V_J = 0.01c$, the electron pressure (P_p), the magnetic pressure (P_{Mp}), and the total pressure (P_{tot_p}) of the condensed region. The ambient pressure, P_0, is also shown. We have at $t = 0$, $q = 0.30$ and $P_0 = 5 \times 10^{-11}$ dynes cm^{-2} and at $t = 1 \times 10^7$ yr, $P_0 = 7.5 \times 10^{-11}$ dynes cm^{-2}. We find that in the integrated space interval, the ratio of the electron pressure of the perturbed region to the ambient region (P_p/P_0) varies slowly from 0.97 to 0.60 for $V_J = 0.01c$, and from 0.97 to 1.0 for $V_J = 0.033c$. The corresponding P_{tot_p}/P_{tot_0} varies from 1 to ~ 0.79 for $V_J = 0.01c$, and $P_{tot_p}/P_{tot_0} \sim 1$ for the space interval considered for $V_J = 0.033c$. These values show that the condensation is increasing approximately under isobaric conditions, as in Cen A. We used equation (7) to estimate the ratio $L_{sp}/\bar{L}_{s0}$ for Cyg A lobes. For $V_J = 0.01c$, for example, at $z \cong 1 \times 10^{23}$ cm (for which $\rho_p/\rho_0 = 4.8$
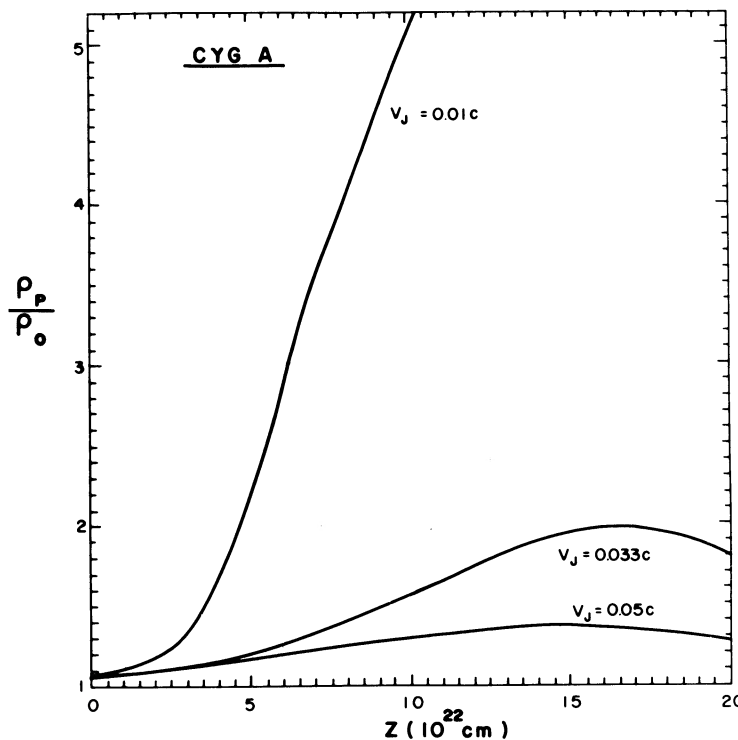
FIG. 6.—Evolution of the total density contrast $\rho_p/\rho_0 (\equiv [\rho_1(r, t) + \rho_0(t)/\rho_0(t)])$ in the radio lobe of Cyg A as a function of the distance ($z = V_J t$) from the origin of the integration for $V_J = 0.01c, 0.033c$, and $0.05c$.
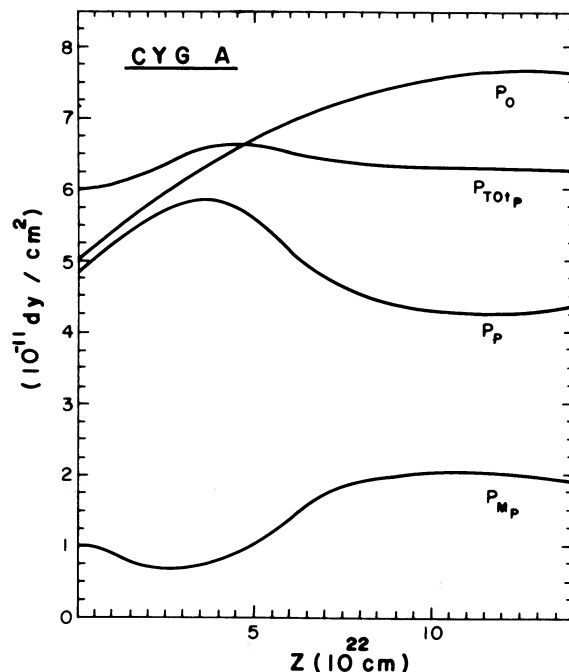
FIG. 7.—Comparison of the electronic pressure (P_p) the magnetic pressure (P_{Mp}), and the total pressure (P_{tot_p}) of the perturbed region in the radio lobe of Cyg A as a function of the distance ($z = V_J t$) from the origin of integration. The ambient pressure, P_0, is also shown.

and $P_p/P_0 = 0.62$) we found from equation (7), $L_{sp}/\bar{L}_{s0} = 3.3$–15 and at $z \cong 6.3 \times 10^{22}$ cm ($t \cong 6.6 \times 10^6$ yr) (for which $\rho_p/\rho_0 = 2.9$ and $P_p/P_0 = 0.73$), we found $L_{sp}/\bar{L}_{s0} = 2.6$–10.6 (for $F = 0.5$–0.1). For $V_J = 0.033c$, at $z = 1.6 \times 10^{23}$ cm (and $t \cong 5.1 \times 10^6$ yr), $\rho_p/\rho_0 = 2$, and $P_p/P_0 = 0.99$, implying $L_{sp}/\bar{L}_{s0} = 2.9$–10.8 (for $F = 0.5$–0.1).

Using minimum energy considerations and the radio data, Perley, Dreher, and Cowan (1984) obtained an equipartition magnetic field for the filaments, $B_{eq_f} \cong 1.3 \times 10^{-4}$ G and for the fainter regions of the jet $\bar{B}_{eq_0} \cong 9 \times 10^{-5}$ G. Using the relations for equipartition (Burns, Owen, and Rudnick 1979), we have that the average radio volume emissivity is $l/V = (B_{eq}^{7/2}\phi)/[2\pi(1+k)C_{12}]$ and the radio volume emissivity of the region of interest (e.g., the filaments): $l/V\phi = B_{eq}^{7/2}/[2\pi(1+k)C_{12}]$, where C_{12} depends on the upper and lower frequency cutoffs and the spectral index of the radio spectrum, k is the ratio between the electron and proton energies, ϕ is the filling factor, V is the volume observed, and l is the radio luminosity. These relations imply that the observed ratio of the volume emissivity of the filaments and adjacent ambient region is $L_{sp}/\bar{L}_{s0} \cong (B_{eq_f}/\bar{B}_{eq_0})^{7/2}$. Using the values of B_{eq_f} and $\bar{B}_{eq_0}$ quoted above, we obtain $L_{sp}/\bar{L}_{s0} \sim 4$ for the Cyg A filaments (again noting, however, that there is a great uncertainty in this value). The above results, again indicate that the thermal instability appears to be sufficient to explain the observed filaments in Cyg A, with $F \lesssim 0.5$.

VI. CONCLUSIONS

We found that the maximum value of $q \equiv V_A^2/V_S^2$, under isobaric conditions for the thermal instability in ERS, is $q_0 = [-2v_e + (3/4\tau_c)(2\eta - 1)]/[(2v_e/3) + (2/\tau_c)]$.

We also found that the nonlinear density contrast is approximately independent of the magnitude of the initial perturbation [tested for $\epsilon = \hat{\rho}_1(0)/\rho_0(0) = \hat{B}_1(0)/B_0(0) = 0.05, 0.1, 0.2$ and 0.3], and the inferred energy loss contrasts are approximately independent of existing inverse Compton losses. This latter result can be compared with calculations in the linear regime where inverse Compton losses strongly suppress the growth of the thermal instability.

Using the results of the previous section, our replies to the questions posed at the end of § I are the following:

1. The luminosities, pressures, and expansion rates indicated by observations of the radio inner jet of Cen A and the radio lobe of Cyg A suggest that the physical parameters of the plasma are propitious for creating a thermal instability (i.e., starting calculations from the condition of marginal stability [eq. (46)], we obtained for the Cen A jet a maximum thermal instability in a distance comparable to the observed distances between the knots and streamers, and for Cyg A a saturated thermal instability in a distance comparable to the distance between the entrance of the jet into the radio lobe and the observed filaments, with a jet velocity $0.01 \le V_J < 0.05c$).

2. The thermal instabilities in Cen A and Cyg A appear to be sufficiently strong to explain the observed filaments by Clarke, Burns, and Feigelson (1986) and Perley, Dreher, and Cowan (1984).

3. Small initial perturbations such as $\epsilon = \hat{\rho}_1(0)/\rho_0(0) = \hat{B}_1(0)/B_0(0) \le 0.1$ can grow in the thermal instability for the observed physical parameters of Cen A and Cyg A.

4. Nonlinear calculations of Cen A and Cyg A indicate density contrasts $\rho_p/\rho_0 \sim 2$–8 for developed thermal instabilities.

It is to be noted that what is discussed in the present paper is a monoenergetic electron spectrum. It is of interest to compare the results of the present paper with observations at a given frequency (e.g., radio) of a power-law spectrum. The condensed region

FILAMENTS IN EXTENDED RADIO SOURCES

formed by the synchrotron thermal instability can appear bright or can appear dark (Eilek 1988). If the condensed region has a high spectral index and emits primarily below the radio region, then it will appear dark at a radio frequency. If, on the other hand, it has a spectral index comparable to the ambient region, then it will appear bright. The exact spectrum of the condensed region depends on the G-function, about which little is known. In particular, we do not know whether the G-function primarily accelerates high-energy electrons, or accelerates electrons independent of energy.

Of particular interest to observers, a given filament could appear bright at a lower frequency.

There is the possibility, however, that after the condensations is formed by the thermal instability (independent of whether it had a high spectral index or a relatively flat spectrum), it is brightened due to the interaction with the ambient medium. In this case it will appear bright at all frequencies.

REFERENCES

Bridle, A., and Perley, R. 1984, *Ann. Rev. Astr. Ap.*, **22**, 319.
Brodie, J., and Bowyer, S. 1985, *Ap. J.*, **292**, 447.
Brodie, J., Königl, A., and Bowyer, S. 1983, *Ap. J.*, **273**, 154.
Burns, J. O., Feigelson, E. B., and Schreier, E. J. 1983, *Ap. J.*, **273**, 128.
Burns, J. O., Owen, F. N., and Rudnick, L. 1979, *A.J.*, **84**, 1683.
Clarke, D. A., Burns, J. O., and Feigelson, E. B. 1986, *Ap. J. (Letters)*, **300**, L41.
de Young, D. S. 1976, *Ann. Rev. Astr. Ap.*, **14**, 447.
Dreher, J. W. 1985, in *Proc. 9th NRAO Workshop*, ed. A. H. Bridle and J. A. Eilek (Greenbank, NC: NRAO), p. 109.
Dreher, J. W., Carrilli, C. L., and Perley, R. A. 1987, *Ap. J.*, **316**, 611.
Eilek, J. 1988, private communication.
Eilek, J., and Caroff, L. J. 1979, *Ap. J.*, **233**, 463.
Eilek, J., and Henriksen, R. N. 1984, *Ap. J.*, **277**, 820.
Feigelson, E. D., Schreier, E. J., Delvaille, J. P., Giaconi, R., Grindley, J. E. and Lightman, A. P. 1981, *Ap. J.*, **251**, 31.
Field, G. B. 1965, *Ap. J.*, **142**, 531.
Gouveia Dal Pino, E. M., and Opher, R. 1989, in preparation.
Hargrave, P. J., and Ryle, M. 1974, *M.N.R.A.S.*, **166**, 305.
Marscher, A. P. 1980, *Ap. J.*, **239**, 296.
Pelletier, G., and Roland, I. 1986, *Astr. Ap.*, **163**, 9.
Perley, R. A., Dreher, J. W., and Cowan, J. J. 1984, *Ap. J. (Letters)*, **285**, L35.
Schreier, E. J., Gorenstein, P., and Feigelson, E. D. 1982, *Ap. J.*, **261**, 42.
Simon, M., and Axford, W. I. 1967, *Ap. J.*, **150**, 105.
Stocke, J., Rieke, G. H., and Lebofsky, M. J. 1981, *Nature*, **294**, 319.
Winter, A. J. B., *et al.* 1980, *M.N.R.A.S.*, **192**, 931.

ELISABETE M. DE GOUVEIA DAL PINO AND REUVEN OPHER: Instituto Astronômico e Geofísico, Universidade de São Paulo, Av. Miguel Stéfano, 4200, Parque do Estado, 04301—São Paulo—SP, Brazil